INTERNATIONAL JOURNAL FOR NUMERICAL METHODS IN FLUIDS, VOL. 15, 1213–1237 (1992)

GENERALIZATION OF PHYSICAL COMPONENT BOUNDARY FITTED CO-ORDINATE (PCBFC) METHOD FOR THE ANALYSIS OF FREE-SURFACE FLOW

AKIHIKO TAKIZAWA*

Nuclear Power R&D Center, the Tokyo Electric Power Company, 1-3, Uchisaiwaicho 1-chome, Chiyoda-ku, Tokyo 100, Japan

SEIICHI KOSHIZUKA

Nuclear Engineering Research Laboratory, the University of Tokyo, 2-22 Shirane, Shirakata, Tokai-mura, Naka-gun, Ibaraki-ken 319-11, Japan

AND

SHUNSUKE KONDO

Department of Nuclear Engineering, Faculty of Engineering, the University of Tokyo, 3-1, Hongo 7-chome, Bunkyou-ku, Tokyo 113, Japan

SUMMARY

This paper presents a systematic and theoretically consistent approach for the analysis of free-surface flow, making use of a number of established ideas such as physical component, boundary-fitted co-ordinate (BFC) and Lagrangian front tracking. The approach extends, theoretically as well as numerically, the use of physical component to general non-orthogonal moving grids and provides a numerically stable BFC method with little labour of free-surface positioning, grid generation and grid renewal. The approach conserves mass even at the free surface and allows time step of the order of the Coulant number. The main body of the present paper starts with the definition of analytical space and Riemannian geometry intrinsic to the physical component by applying to it the theorems of differential geometry and manifold theory. Then the governing equations of flow and free surface for the physical component are defined in the general 3D form with the notation of the new Riemannian geometry.Numerical procedures and the fully discrete equations are also presented for the benefit of potential users. Finally, several 2D examples demonstrate the basic performance of the present method by showing the computability of complex free-surface motion.

KEY WORDS Physical component Lie derivative Physical curvilinear space Riemannian geometry Lagrangian front tracking Free surface

1. INTRODUCTION

Free-surface flow is one of the common states of incompressible fluid, and its study is important for a deeper understanding of fluid physics. Since free-surface flow is often dynamic and exact experimental measurement of the flow and pressure is difficult, contribution of numerical method is important for the investigation and, for quantitative investigation, the method should be able to handle the movement of free surface as precisely as flow. From the viewpoint of numerical

* Also research student in the University of Tokyo.

0271–2091/92/221213–25$17.50

Received 25 November 1991
Revised 4 May 1992

analysis, free-surface flow is unique in the following two points. First, it is a problem of moving boundary. Second, movement of the boundary is not prescribed; free surface is a boundary coupled with flow and is to be obtained as a solution of analysis. The existing numerical methods for analysing free-surface flow are classified into two groups according to the method of free-surface tracking. One of them employs direct Lagrangian tracking with moving boundaries and the other employs indirect tracking with fixed grid system. In the latter method, the free-surface is determined by a distribution of volume of fluid (VOF)[1] in each cell, but this method has setbacks of poor mass conservation, large numerical viscosity at the free surface and reduced time step for the convergence of VOF value. Low reliability of free surface hurts even the reliability of flow.

On the other hand, the analytical method with Lagrangian free-surface tracking requires flexible grids for analysis. Most of the numerical methods with Lagrangian free-surface tracking are based on one of the following numerical techniques: the finite element method (FEM),[2] the boundary element method (BEM)[3] and the boundary-fitted co-ordinate (BFC)[4] method. Among them the BFC method is chosen in the present study because the well-developed techniques of the finite difference (FD) method are applicable and the analytical method can be formulated based on the strict mathematical tool of Riemannian geometry. One of the problem in applying the techniques of conventional FD method on the curved grid system of the BFC method is that there is a discrepancy between the direction of the local grids and that of the Euclidean rectangular co-ordinates with which the physical space is defined. In the BFC method formulated based on Riemannian geometry with contravariant or covariant vectors as variables, this problem is overcome by a mapping from the physical space to the curvilinear space of which grid system is regular and follows the direction of rectangular co-ordinates. In other words, shapes of the boundaries are deformed for the convenience of computation in this type of BFC method. But the mapping not only deforms boundaries but also transforms flow variables to their contravariant (or covariant) counterparts, and the transformation changes not only the direction of flow variables but also its magnitude to be inversely proportional to the scale factor of the mesh $h_i = \sqrt{g_{ii}}$. The change of direction is convenient to the analysis but the change of magnitude is *not*, since the scale factor varies cell to cell and this induces undesirable mesh sensitivities. This sensitivity, however, can be cancelled by the use of physical component.

Physical component was first introduced by Truesdell[5] as an attempt to give vectors and tensors the natural physical dimensions and immediate physical meanings that were lost by tensor transformation. He defined the physical component of contravariant vectors by multiplying with them the scale factors of the mesh $h_i = \sqrt{g_{ii}}$. He even derived the connection coefficients (Christoffel symbols) and covariant derivatives of physical components, but only for the case of orthogonal co-ordinates. If restricted to the orthogonal co-ordinates, these coefficients can be derived from their non-physical counterparts by a simple multiplication of scale factors.

Then, researchers like Pope[6] and Ryskin and Leal[7,8] introduced physical component into the analysis of incompressible fluid flow that is bounded by complex boundaries. However, their principal purpose of the introduction was just the simplification of expression of governing equations and the resulting discretizations. They restricted the use of physical component to the orthogonal grids, and suffered inconveniences that complex boundaries distorted the whole inside mesh and changed the mesh size by orders. They paid much effort on the generation of orthogonal grid systems, but little on the extension of physical component to the general non-orthogonal grids.

Following these studies, Demirdzic *et al.*[9] made progress in the use of physical component. First, they used it to reduce undesirable mesh sensitivities. Second, they extended the use to general non-orthogonal grids. Although it had been long believed that the physical component is

useful only in the case of orthogonal co-ordinates, they released it from the restriction of orthogonality.

Koshizuka *et al.*[10–12] also adopted physical component to the BFC method to promote numerical stability. They showed, theoretically as well as numerically, that only the physical component converges when the mesh size of the adjacent cells differs more than three times.[13] They also clarified the geometrical meaning of the quantities of physical component and extended a number of differencing techniques of FD, such as the staggered arrangement and the MAC (marker and cell) algorithm, to the BFC method.

Achievements of these two research groups provide numerically stable method to analyse the flow in complex boundaries using 'sound' grid systems, with little labour of mesh generation and relatively large time step. Their progress is also important for the analysis of free-surface flow; free surface is susceptible to numerical stability, control of mesh size in the moving boundary problem is often difficult, and movement of the whole inside mesh induced by the movement of free surface can hurt the reliability of the result computation.

To extend the use of physical component BFC (PCBFC) method to the analysis of free surface flow, we need a new function for assessing the effects of grid movement on variables. Flow vectors suffer change not only by grid displacement but also by grid rotation, and each effect we are to assess in the curved co-ordinate system. This is a very complex process if we do not use the Lie derivative. The Lie derivative is a co-ordinate-free derivative along a curved line, and was first introduced into the fluid flow analysis by Ogawa and Ishiguro.[14] They analysed with the Lie derivative some incompressible flows bounded by prescribed moving boundaries using non-physical contravariant flow vectors as variables. To introduce the Lie derivative into the formulation with physical components as variables, we need a 'physical component counterpart of the Lie derivative.' However, contrary to the preceding works, a simple substitution of physical component into the formula of the Lie derivative written in the non-physical form does not work, since the Lie derivative $L_V u^i$ requires the replacements of not only u^i, the flow vectors, but also of V, the direction of movement, to their physical component counterparts. To obtain this derivative in the form of physical component, we must apply the theorems of Riemanian geometry from the beginning, and to apply these theorems the basic quantities of physical component such as metrics, connections and covariant derivatives should be reviewed first, not as physical component counterparts but as *proper* geometrical objects that belong to their own analytical space and Riemannian geometry. Differential geometry and manifold theory inform us that each set of tensor components has its own space and geometry. This paper provides a deeper insight into the significance of physical component, and is important in the analysis with fixed boundaries as well. The primitive concept of this paper has been presented by Takizawa and Kondo[15] in a local conference.

The objective of the present paper is to provide a viable and theoretically consistent approach for the simulation of free-surface flow based on the development of a new analytical space and a new Riemannian geometry intrinsic to the physical component. We start with the development of mathematical foundation. In Section 2 we define a space, Riemannian geometry and derivatives that are intrinsic to the physical component. We also derive some useful relations of the connection coefficients based on the characters of the space of physical component in this section. In Section 3 we formulate the governing equations of free surface flow in the general 3D form with the notation of the Riemannian geometry. In Section 4 we discuss about the differencing techniques, the computational algorithm and the initial and boundary conditions in detail. In Section 5 we show some numerical examples. Although the formulation is carried out in the general 3D form, examples shown in this section are performed in 2D because the principal objective of the present paper is the theoretical development and demonstration of the basic

performance. We will analyse three different bench-mark problems of flow in a cacity: (1) periodical free-surface motion induced by external excitation, (2) free-surface motion induced by forced circulation, and (3) complex free-surface motion induced by a superposition of external excitation and forced circulation. A summary of differential geometry and manifold theory used in the main body of the present paper is given in the Appendix.

2. MATHEMATICAL FOUNDATION

In this section we lay down the mathematical foundation of the PCBFC method in the general 3D form through the introduction of analytical space and Riemannian geometry of the physical component (RGPC). Throughout this paper, equations are described with index notation and the summation convention of tensor calculus. A Roman letter index is an index of 3-space ($i=1$–3), t is an index of time ($t=4$) and a Greek letter is an index of 4-spacetime ($\imath=1$–4). An index in parentheses denotes physical component.

2.1. Space of physical component

Contravariant unit tangents of the curvilinear space are defined as follows:

$$\partial\xi^i_{[j]}=\frac{\delta^i_j}{\sqrt{g_{jj}}}, \tag{1}$$

where ξ^i, $\sqrt{g_{ii}}$ and δ^i_j are the co-ordinate of curvilinear space, scale factor of the mesh and the Kronecker delta, respectively, and suffix $[j]$ denotes the jth component. Physical component of the contravariant vector u^i is defined as follows:

$$u^{(i)}=\sqrt{(g_{ii})}u^i. \tag{2}$$

Although the standard textbooks of tensor calculus[16] state that the physical components do not transform as tensors, they do if we introduce a new space $\{\xi^{(i)}\}$ by modifying the contravariant unit tangents of equation (1) in the following way:

$$\partial\xi^{(i)}_{[j]}=\delta^i_j. \tag{3}$$

Equations (1)–(3) give the following relation on $u^{(i)}$ and u^i.

$$u^{(i)}=\frac{\partial\xi^{(i)}}{\partial\xi^j}u^j. \tag{4}$$

This equation indicates that the physical components are tensors of a space defined by the co-ordinates $\{\xi^{(i)}\}$.

The co-ordinates $\{\xi^{(i)}\}$ are curvilinear just as the co-ordinates $\{\xi^i\}$, but the lengths of the unit tangents are all unity, which indicates that the space defined by $\{\xi^{(i)}\}$ is identical to the physical space. We call this space 'physical curvilinear space (PCS). The PCS is illustrated in Figure 1 along with other spaces. Different from the curvilinear space, the discrepancy between the direction of grids and that of the co-ordinates (see Section 1) is overcome by the deformation of the co-ordinates, and there is no deformation of flow boundaries by a mapping from the physical space to the PCS. It can be said that the physical component is less sensitive to the analytical mesh size because the space of analysis suffers no deformation by the mapping.

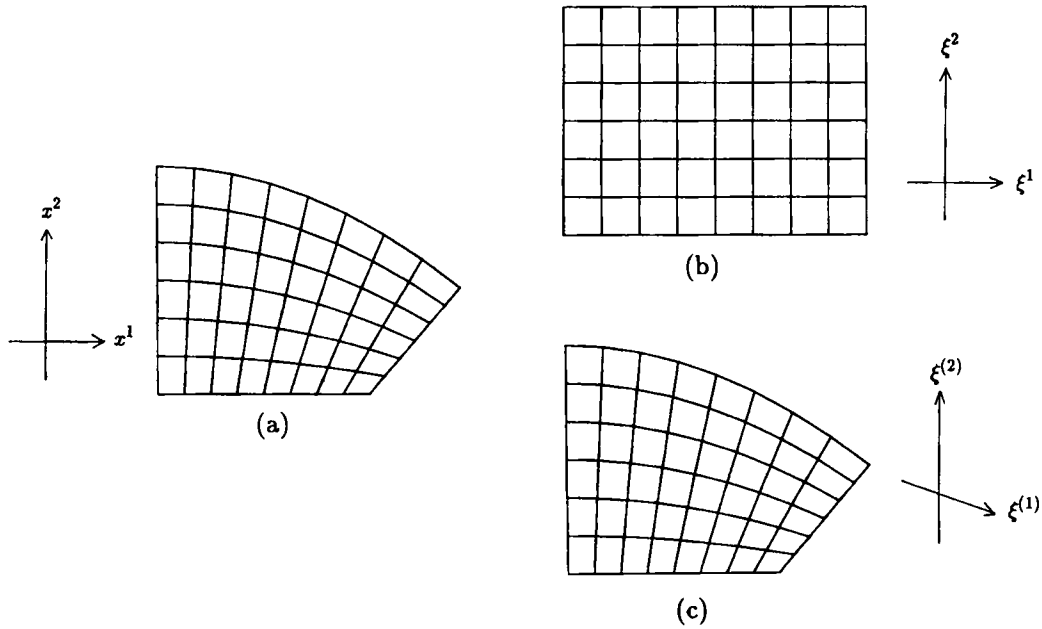

Figure 1. Analytical spaces and the co-ordinates used in the BFC method: (a) physical space; (b) curvilinear space; (c) physical curvilinear space

2.2. *Riemannian geometry of physical component*

Now that the PCS has been defined, we can derive the RGPC by applying the theorems of differential geometry and manifold theory (see the Appendix) to the PCS. Jacobian, metrics and connection coefficients are the important geometrical quantities in the PCBFC method, corresponding to the element of cell volume, unit length, and the curvatures of the co-ordinates, respectively. These quantities are obtained from the transformation matrix of the mapping from the PCS to the physical space defined as follows:

$$T=[T^x_{(\xi)}]=\left(\frac{\partial x^j}{\partial \xi^{(i)}}\right)=[x^j_{(i)}]=[\cos\theta_{ji}], \tag{5}$$

where $\{x^i\}$, $x^j_{(i)}$, $T^x_{(\xi)}$ and θ_{ji} denote the co-ordinate of physical space, partial derivative of x^j with respect to $\xi^{(j)}$, members of the transformation matrix T, and the angle formed by the $\xi^{(i)}$ axis and the x^j axis, respectively. Jacobian is a determinant of T:

$$J=|T|. \tag{6}$$

Metrics are obtained by substituting $T^x_{(\xi)}$ in equation (5) and the trivial metrics of physical space given in equation (58) into equation (56) and are given as follows:

$$g_{(ii)}=1, \qquad g_{(ij)}=\cos\alpha_{ij}, \tag{7}$$

where α_{ij} is the angle formed by $\xi^{(i)}$ and $\xi^{(j)}$ axes. In other words metrics are the inner products of the unit tangents of PCS.

Connection coefficients of the PCS are obtained by substituting $T^x_{(\xi)}$ of equation (5) and the trivial connections of physical space of equation (67) into equation (62). For example, $\Gamma^{(3)}_{(12)}$ is

given as follows:

$$\Gamma^{(3)}_{(12)}=\frac{1}{J}\begin{vmatrix} x_{(1)} & x_{(2)} & x_{(21)} \\ y_{(1)} & y_{(2)} & y_{(21)} \\ z_{(1)} & z_{(2)} & z_{(21)} \end{vmatrix}, \tag{8}$$

where $x_{(ji)}$ denotes $\partial_{(i)}(\partial_{(j)}x)$. In general, $\Gamma^{(i)}_{(jk)}$ can be obtained as a determinant of T whose members in the ith column are replaced with $\{x_{(kj)}, y_{(kj)}, z_{(kj)}\}$, to be divided by J. Higher-order differentials in the PCS depend on the order of differentiation (uncommutative), as indicated by the following inequality:

$$\partial_{(i)}\partial_{(j)}f=\frac{1}{\sqrt{g_{ii}}}\partial_i\left(\frac{1}{\sqrt{g_{jj}}}\partial_j\right)f\neq\frac{1}{\sqrt{g_{jj}}}\partial_j\left(\frac{1}{\sqrt{g_{ii}}}\partial_i\right)f=\partial_{(j)}\partial_{(i)}f. \tag{9}$$

From this inequality, we can obtain another inequality concerning the connection coefficients:

$$\Gamma^{(i)}_{(jk)}\neq\Gamma^{(i)}_{(kj)}. \tag{10}$$

This inequality indicates that the PCS has non-zero torsion (see Section A.6). In a strict sense, this inequality excludes the RGPC from Riemannian geometry, but we call it 'Riemannian geometry' by slightly extending the definition.

2.3. Derivatives of physical component

There are two co-ordinate-free derivatives used in the PCBFC method; covariant derivatives and Lie derivatives. Covariant derivative is a co-ordinate-free partial derivative (see Section A.2). Covariant derivative of $u^{(i)}$ with respect to $\xi^{(j)}$ is defined as follows:

$$\nabla_{(j)}u^{(i)}=\frac{\partial u^{(i)}}{\partial\xi^{(j)}}+\Gamma^{(i)}_{(jk)}u^{(k)}, \tag{11a}$$

where the second term on the right-hand side of the equation serves for the correction of direction change of the curved PCS co-ordinates. Covariant derivative of a scalar p is defined as follows:

$$\nabla_{(i)}p=\frac{\partial p}{\partial\xi^{(i)}}, \tag{11b}$$

where there is no correction term because scalar has no directional element.

Lie derivative is a co-ordinate-free total derivative. Standard textbooks of differential geometry[17,18] inform that the Lie derivative of $u^{(i)}$ in the direction of V is expanded as follows (see Section A.4):

$$\mathrm{L}_V u^{(i)}=V^{(j)}\nabla_{(j)}u^{(i)}-u^{(j)}\nabla_{(j)}V^{(i)}. \tag{12a}$$

The first term on the right-hand side of equation (12a) represents the effect of grid displacement, while the second term represents the effect of grid rotation. The Lie derivative of p is written as follows:

$$\mathrm{L}_V p=V^{(j)}\nabla_{(j)}p=V^{(j)}\frac{\partial p}{\partial\xi^{(i)}}, \tag{12b}$$

where there is no rotation term because scalar has no directional element.

Although equation (12a) is written with physical components, the rotation coefficients $\nabla_{(j)}V^{(i)}$ may have non-zero values even when the grid moves in parallel. This mesh sensitivity is

outstanding especially when the mesh movement changes the intervals of mesh; so, this sensitivity is similar to that occurring in the non-physicals, referred to in Section 1. To have a numerically stable free surface, we should improve equation (12a) to fit the physical component, and for the improvement we need to grasp the PCS as an entity of 4-spacetime instead of a combination of 3-space and time. In the 4-spacetime, the time axis is normal to the 3-space so that it keeps the meaning of 'global time' and requires no modification of the formulae of 3-space obtained so far.

The improvement starts with an expression of evolution equation in the physical space. Given an evolution function f, the evolution of the system is described as follows:

$$\frac{\partial u^{(i)}}{\partial t}=f(u^i, \partial_j u^i, p). \tag{13}$$

In the 4-spacetime, equation (13) is written as follows:

$$\nabla_t u^{(i)}=f(u^{(i)}, \nabla_{(j)} u^{(i)}, p),$$

where ∇_t is a covariant derivative with respect to time. The above equation can be expanded as follows:

$$\frac{\partial u^{(i)}}{\partial t}=f(u^{(i)}, \nabla_{(j)} u^{(i)}, p)-\Gamma^{(i)}_{(tj)} u^{(j)}.$$

The above equation advances time without moving the point of definition because the time axis is normal to the 3-space and the advancement along the time axis does not change the point of definition even when there is a grid displacement. So, to adjust the point of definition, we need to add one more term $\nabla_V u^{(i)}$ that assesses the change of $u^{(i)}$ caused by a parallel displacement in the direction of V, and this derivative is expanded as follows:

$$\nabla_V u^{(i)}=V^{(j)}\nabla_{(j)} u^{(i)}. \tag{14}$$

Then the evolution equation in the PCS is obtained in the following form:

$$\frac{\partial u^{(i)}}{\partial t}=f(u^{(i)}, \nabla_{(j)} u^{(i)}, p)-\Gamma^{(i)}_{(tj)} u^{(j)}+V^{(j)}\nabla_{(j)} u^{(i)}. \tag{15}$$

A comparison of equations (13) and (15) indicates that the last two terms on the right-hand side of equation (15) serve as the Lie derivative. We have, therefore, obtained an improved mesh-insensitive Lie derivative for the PCBFC method, written as follows:

$$\mathrm{L}_V u^{(i)}=V^{(j)}\nabla_{(j)} u^{(i)}-\Gamma^{(i)}_{(tj)} u^{(j)}. \tag{12c}$$

Time connection coefficients $\Gamma^{(i)}_{(jk)}$ in equation (12c) can be obtained in the same manner as the space connection coefficients in equation (8). For example, $\Gamma^{(3)}_{(t2)}$ is given in the following form:

$$\Gamma^{(3)}_{(t2)}=\frac{1}{J}\begin{vmatrix} x_{(1)} & x_{(2)} & x_{(2t)} \\ y_{(1)} & y_{(2)} & y_{(2t)} \\ z_{(1)} & z_{(2)} & z_{(2t)} \end{vmatrix} \tag{16}$$

2.4 Relations of the connection coefficients

The characters of the PCS give some relations of the connection coefficients. First, the space co-ordinates of the PCS have foliated structures[19] (see Section A.7). A small circuit drawn along

the co-ordinates on a certain leaf of the PCS remains in that leaf. This indicates that the element of the torsion tensor of PCS that stands out of the leaf vanishes:

$$T^{(i)}_{(jk)} = \Gamma^{(i)}_{(jk)} - \Gamma^{(i)}_{(kj)} = 0 \quad (\text{if } i \neq j \neq k \neq i). \tag{17}$$

The above equation immediately gives the following relation of the connection coefficients:

$$\Gamma^{(i)}_{(jk)} = \Gamma^{(i)}_{(kj)} \qquad (\text{if } i \neq j \neq k \neq i) \tag{18}$$

Equation (18) overrides equation (10). The time axis is not foliated and equation like equation (18) never holds, but the following relations hold since the time axis is normal to the 3-space:

$$\Gamma^{(i)}_{(jt)} = 0, \qquad \Gamma^{(t)}_{(ij)} = 0. \tag{19}$$

Second, connections of the PCS are metrical (see Section A.5), i.e.

$$\nabla_{(k)} g_{(ij)} = 0. \tag{20}$$

The above equation is written explicitly as follows:

$$\partial_{(k)} g_{(ij)} - \Gamma^{(r)}_{(ki)} g_{(rj)} - \Gamma^{(r)}_{(kj)} g_{(ir)} = 0.$$

Taking the case of $i=j$ and using equation (7), the above equation reduces to the following form:

$$g_{(ir)} \Gamma^{(r)}_{(ji)} = 0,$$

or, more explicitly, using equation (7) again, it is written as follows:

$$\cos \alpha_{ir} \Gamma^{(r)}_{(ji)} = 0.$$

The above equation can be evolved, for example, in the following form:

$$\Gamma^{(1)}_{(j1)} = -\cos \alpha_{12} \Gamma^{(2)}_{(j1)} - \cos \alpha_{13} \Gamma^{(3)}_{(j1)}. \tag{21a}$$

Equation (65) indicates that $\{\Gamma^{(i)}_{(jk)}\}$ $(i=1\text{–}3)$ are the curvature vectors of $\xi^{(j)}$ axis when moved along the $\xi^{(k)}$ axis. Since curvature vector of a curve is normal to the tangent of the curve, $\Gamma^{(i)}_{(jk)}$ $(i=k)$ vanishes if the local co-ordinates are orthogonal. But as the co-ordinates are oblique, $\Gamma^{(i)}_{(jk)}$ $(i=k)$ gains component by decomposition as described in Equation (21a).

The same relation holds in the time connection coefficients. For example, the following equation holds:

$$\Gamma^{(1)}_{(t1)} = -\cos \alpha_{12} \Gamma^{(2)}_{(t1)} - \cos \alpha_{13} \Gamma^{(3)}_{(t1)}. \tag{21b}$$

Relation like equation (21b) never holds in the imperfect rotation coefficients expressed by $\nabla_{(j)} V^{(i)}$. So, equation (21b) indicates that the non-physical element has been completely removed from the present formulation.

Substitution of equation (8) into equation (79) shows that the PCS is a flat space (total-curvature-free). Substitution of metrics in equation (7) into equation (57a) show that the metrics are equivalent to the second cosine formula of the plain trigonometry. These facts indicate that the RGPC is a natural extension of Euclidean geometry.

3. GOVERNING EQUATIONS

In this section we define the governing equations of flow and free surface in the form of the PCBFC method.

3.1. Flow

The flow is governed by the equation of continuity and the Navier–Stokes equation of incompressible fluid. These equations in the form of the PCS are obtained from those in the physical space by replacing the partial derivatives with the covariant derivatives of the PCS, and are given, respectively, as follows:

$$\nabla_{(i)}u^{(i)}=0, \tag{22a}$$

and

$$\frac{\partial u^{(i)}}{\partial t}=-u^{(j)}\nabla_{(j)}u^{(i)}-\frac{1}{\rho}g^{(ik)}\nabla_{(k)}p+\nu\nabla_{(j)}g^{(jk)}\nabla_{(k)}u^{(i)}+f_l g^{(ij)}\nabla_{(j)}x^l, \tag{23a}$$

where ρ, ν and f_l are the density, viscosity and the constant of external forces (gravity and external excitation), respectively, and the summation runs over l.

For the convenience of computation, we rewrite equation (22a) in the following form:

$$\frac{h_i}{V}\partial_{(i)}\left(\frac{V}{h_i}u^{(i)}\right)=0, \tag{22b}$$

where V and h_i $(=\sqrt{g_{ii}})$ are the volume of the analytical cell and the length of the cell side, respectively, and there is no summation over i without parenthesis. The above equation is obtained from the counterpart in the curvilinear space, in which V and h_i are the Jacobian and the metric, respectively. In equation (22b), $V/d_{(i)}$ is the cross-section of cell that faces the flow vector $v^{(i)}$, and $Vu^{(i)}/d_{(i)}$ denotes the flux of flow. In the same manner we also rewrite equation (23a) in the following form:

$$\frac{\partial u^{(i)}}{\partial t}=-u^{(j)}\nabla_{(j)}u^{(i)}-\frac{1}{\rho}g^{(ik)}\nabla_{(k)}p+\nu\left[\frac{h_j}{V}\partial_{(j)}\left(\frac{V}{h_i}g^{(jk)}\tau^{(i)}_{(k)}\right)+\Gamma^{(i)}_{(jl)}g^{(jk)}\tau^{(l)}_{(k)}\right]+f_l g^{(ij)}\nabla_{(j)}x^l, \tag{23b}$$

where the diffusion term has been rewritten and $\tau^{(l)}_{(k)}$ is a stress tensor defined as follows:

$$\tau^{(j)}_{(i)}=\nabla_{(i)}u^{(j)}. \tag{24}$$

3.2. Free surface

The movement of the free surface is governed by the pressure condition and the kinematic condition. In the present method the free surface is tracked by a certain 'leaf', a plane that consists of co-ordinate axes of the PCS (see Section A.7).

The pressure condition is fulfilled simply by putting $p=0$ at the surface leaf of the PCS, and no interpolation as required in the indirect tracking method is necessary. Surface tension is not incorporated yet, and we deal only with problems with small free-surface curvatures.

The kinematic condition is written in the physical space as follows:

$$\frac{\mathrm{D}F}{\mathrm{D}t}=0, \tag{25a}$$

where D and F are, respectively, the Lagrangian derivative and 'surface function', that is constant on the free surface. First, we convert equation (25a) in the form of PCS. From the expression of the Lagrangian derivative in the physical space,

$$\frac{\mathrm{D}}{\mathrm{D}t}=\frac{\partial}{\partial t}+u^i\frac{\partial}{\partial x^i}, \tag{26a}$$

we can obtain its form in the 4-spacetime of PCS as follows:

$$\frac{\mathrm{D}}{\mathrm{D}t}=u^{(i)}\nabla_{(i)}, \tag{26b}$$

where $u^{(i)}$ is a non-relativistic 4-velocity and $u^{(4)}$ is unity. So, equation (25a) has the following form in the 4-spacetime:

$$u^{(i)}\nabla_{(i)}F=0. \tag{25b}$$

Equation (25b) can be expanded as follows:

$$\frac{\partial F}{\partial t}+u^{(i)}\frac{\partial F}{\partial \xi^{(i)}}=0, \tag{27}$$

where there is no correction term for the direction change of the curved PCS co-ordinates since F is a scalar.

We track the free surface with a certain $\xi^{(1)}$–$\xi^{(2)}$ leaf of the PCS. Since the $\xi^{(1)}$ and $\xi^{(2)}$ axes lie on the free surface and F is constant there, the following equations hold:

$$\frac{\partial F}{\partial \xi^{(1)}}=\frac{\partial F}{\partial \xi^{(2)}}=0 \quad \text{(on the free surface)}. \tag{28}$$

Equation (28) simplifies equation (27) to the following form:

$$\left.\frac{\partial F}{\partial t}\right|_{\xi^{(3)}=\text{constant}}=-u^{(3)}\left.\frac{\partial F}{\partial \xi^{(3)}}\right|_{t=\text{constant}}, \tag{29}$$

which is satisfied by the following relation:

$$\Delta\xi^{(3)}=u^{(3)}*\Delta t. \tag{30}$$

The above equation is fulfilled by simply imposing the equation of continuity on the surface cells. Free-surface positioning is quite simple and requires little computational time in the PCBFC method.

3.3. Movement of the point of definition

The free-surface movement causes grid movement. Velocity $u^{(i)}$ and pressure p after the grid movement in the direction of V are related with those before the grid movement by the Lie derivative in the following way:

$$u^{(i)}(\mathrm{a})=u^{(i)}(\mathrm{b})+\mathrm{L}_V u^{(i)}*\Delta t, \tag{31a}$$

$$p(\mathrm{a})=p(\mathrm{b})+\mathrm{L}_V p*\Delta t, \tag{31b}$$

where (a) and (b) denote 'after' and 'before' the grid movement and Δt is a time step.

4. NUMERICAL PROCEDURE

We present the computational algorithm and full discrete equations in this section. These procedures are developed based on the works of Koshizuka *et al.*[10–12]

4.1. Computational algorithm

The developed code is named 'BELIEF' (a BFC code extended with Lie derivative for the analysis of incompressible fluid flow with free surface). The computational scheme adopted in

BELIEF is an extension of SMAC (simplified marker-and-cell),[20] to which the step for the grid movement and the assessment of its impact is added. The convective scheme used in BELIEF is either the second-order central difference scheme or the first-order upwind difference scheme. Point SOR (successive over-relaxation) method is used to solve the Poisson equation.

Staggered arrangement of variables is chosen for assuring numerical stability as well as the conservation of mass and energy. Flow vector is defined on the cell surface, stress tensor of $i \neq j$ is defined on the cell side, pressure, stress tensor of $i=j$, Jacobian, metric and connection coefficient of $j \neq k$ are defined at the cell centre, and connection coefficient of $j=k$ is defined at the grid point. When these quantities at another point of definition are necessary, averages of those at the nearest points of definition are used.

In estimating connection coefficients, those of $i \neq k$ are estimated first by equations (8) and (16), and after these those of $\Gamma^{(i)}_{(jk)}$ $(i=k)$ by equations (21a) and (21b). By this procedure we can circumvent the cumbersome character of the PCS that differentials of the higher-order depend on the order of differentiation [equation (9)]. This is because only the connection coefficients of $\Gamma^{(i)}_{(jk)}$ $(i=k)$ are susceptible to this uncommutativity, which is shown by substituting connection coefficients of the curvilinear space and transformation matrix from the curvilinear space to the PCS into equation (62). The differentials of the curvilinear space are commutative, the transformation matrix is diagonal and the second term in the parenthesis of the right-hand side of equation (62), which is the origin of uncommutativity, vanishes in the case of $\Gamma^{(i)}_{(jk)}$ $(i \neq k)$.

4.2. *Discretization techniques*

The following discretizations are given in two dimensions and only those of $u^{(1)}$ are presented for simplicity, but extension to the general case is obvious. The pointer (i, j) denotes the cell centre and the pointer $(\bar{i}, j)$ with $\bar{i}=i+1/2$ denotes the cell face where $u^{(1)}_{\bar{i}, j}$ is defined. The cell face $(\bar{i}, j)$ is shared by the cells of (i, j) and $(i+1, j)$.

The computational algorithm consists of three steps: the predictor step of SMAC, the corrector step of SMAC and the grid movement step. We present discrete equations in this order. First step is the derivation of the predictor of flow vectors by explicitly discretizing the four terms in the right-hand side of equation (23b). The predictor is defined on the cell face and the discretizations at $(\bar{i}, j)$ are presented below.

First, the convective term of equation (23b) is expanded as follows:

$$\mathrm{CON}^{(1)} = -(u^{(1)}\nabla_{(1)}u^{(1)} + u^{(2)}\nabla_{(2)}u^{(1)}). \tag{32}$$

It has been shown that the flow vectors may show unrealistic swings by having the influence of centrifugal effects of the curved mesh in advance, unless the connection coefficients in the convective term are discretized at upwind.[10-12] In the present study, whole connection terms are discretized at upwind:

$$\bar{u}^{(1)}_{\bar{i}+1, j} = u^{(1)}_{\bar{i}+1, j} + (\Gamma^{(1)}_{(1k)}u^{(k)})_{\bar{i}+1, j}\Delta\xi^{(1)},$$
$$\bar{u}^{(1)}_{\bar{i}-1, j} = u^{(1)}_{\bar{i}-1, j} - (\Gamma^{(1)}_{(1k)}u^{(k)})_{\bar{i}-1, j}\Delta\xi^{(1)},$$
$$\bar{u}^{(1)}_{\bar{i}, j+1} = u^{(1)}_{\bar{i}, j+1} + (\Gamma^{(1)}_{(2k)}u^{(k)})_{\bar{i}, j+1}\Delta\xi^{(2)},$$

and

$$\bar{u}^{(1)}_{\bar{i}, j-1} = u^{(1)}_{\bar{i}, j-1} - (\Gamma^{(1)}_{(2k)}u^{(k)})_{\bar{i}, j-1}\Delta\xi^{(2)}. \tag{33}$$

Equation (68) indicates that $\bar{u}^{(1)}$'s in the above equations are the flow vectors decomposed by the common co-ordinate system belonging to the flow vector of interest $u^{(1)}_{\bar{i}\bar{j}}$ (see Figure 2). Then the

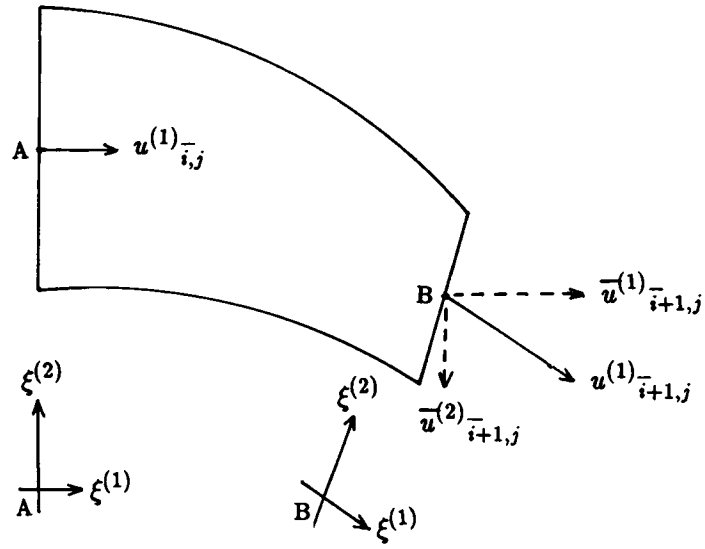

Figure 2. Decomposition of flow vectors by the common co-ordinates (a simple case that flow vectors have only $u^{(1)}$ components is drawn.)

convective term is discretized as follows:

$$\mathrm{CON}^{(1)}=\frac{u^{(1)}_{\bar{i},j}}{2\Delta\xi^{(1)}}[(\bar{u}^{(1)}_{\bar{i}+1,j}-\bar{u}^{(1)}_{\bar{i}-1,j})+\alpha\,\mathrm{sgn}(\bar{u}^{(1)}_{\bar{i},j})(u^{(1)}_{\bar{i}+1,j}-2u^{(1)}_{\bar{i},j}+\bar{u}^{(1)}_{\bar{i}-1,j})]$$
$$+\frac{u^{(2)}_{\bar{i},j}}{2\Delta\xi^{(2)}}\left[(\bar{u}^{(1)}_{\bar{i},j+1}-\bar{u}^{(1)}_{\bar{i},j-1})+\alpha\,\mathrm{sgn}(\bar{u}^{(2)}_{\bar{i}\bar{j}})(u^{(1)}_{\bar{i},j+1}-2uu^{(1)}_{\bar{i},j}+\bar{u}^{(1)}_{\bar{i},j-1})\right], \tag{34}$$

where α is either 0 (central difference scheme) or 1 (upwind difference scheme) and 'sgn' indicates signature. The present discretization technique can be easily extended to another convective schemes.

Second, the pressure term is expanded as follows:

$$\mathrm{PRE}^{(1)}=-\frac{1}{\rho}(g^{(11)}\nabla_{(1)}p+g^{(12)}\nabla_{(12)}p), \tag{35}$$

and is discretized in the following way:

$$\mathrm{PRE}^{(1)}=-\frac{1}{\rho}\left[\frac{g^{(11)}}{\Delta\xi^{(1)}}(p_{i+1,j}-p_{i,j})+\frac{g^{(12)}}{4\Delta\xi^{(2)}}(p_{i+1,j+1}+p_{i,j+1}-p_{i+1,j-1}-p_{i,j-1})\right]. \tag{36}$$

Third, the diffusion term is expanded as follows:

$$\mathrm{DIF}^{(1)}=\nu(\mathrm{DIF1}+\mathrm{DIF2}), \tag{37}$$

where DIF1 and DIF2 are written, respectively, in the following ways:

$$\mathrm{DIF1}=\frac{h_1}{V}\partial_{(1)}\left(\frac{V}{h_1}g^{(11)}\tau^{(1)}_{(1)}\right)+\frac{h_1}{V}\partial_{(1)}\left(\frac{V}{h_1}g^{(12)}\tau^{(1)}_{(2)}\right)$$
$$+\frac{h_2}{V}\partial_{(2)}\left(\frac{V}{h_2}g^{(21)}\tau^{(1)}_{(1)}\right)+\frac{h_2}{V}\partial_{(2)}\left(\frac{V}{h_2}g^{(22)}\tau^{(1)}_{(2)}\right), \tag{38}$$

$$\mathrm{DIF2}=\tau^{(1)}_{(1)}(g^{(11)}\Gamma^{(1)}_{(11)}+g^{(21)}\Gamma^{(1)}_{(21)})+\tau^{(1)}_{(2)}(g^{(12)}\Gamma^{(1)}_{(11)}+g^{(22)}\Gamma^{(1)}_{(21)})$$
$$+\tau^{(2)}_{(1)}(g^{(11)}\Gamma^{(1)}_{(12)}+g^{(21)}\Gamma^{(1)(22)})+\tau^{(2)}_{(2)}(g^{(12)}\Gamma^{(1)}_{(12)}+g^{(22)}\Gamma^{(1)}_{(22)}). \tag{39}$$

Only DIF1 has differentials. The first term on the right-hand side of equation (38) is taken as an example of discretization and is written as follows:

$$\mathrm{DIF1}(1)=\frac{1}{V}\left[\left(\frac{V}{h_1}g^{(11)}\tau^{(1)}_{(1)}\right)_{i+1,j}-\left(\frac{V}{h_1}g^{(11)}\tau^{(1)}_{(1)}\right)_{i,j}\right], \tag{40}$$

since $\Delta\xi^{(1)}=h_1$ holds.

Finally, the external force term is expanded as follows:

$$\mathrm{EXT}^{(1)}=f_1g^{(11)}\nabla_{(1)}x+f_1g^{(12)}\nabla_{(2)}x+f_2g^{(11)}\nabla_{(1)}y+f_2g^{(12)}\nabla_{(2)}y, \tag{41}$$

where x and y are x^1 and x^2, respectively. The first term on the right-hand side of equation (41) is taken as an example of discretization and is written as follows:

$$\mathrm{EXT}(1)=\frac{f_1g^{(11)}}{\Delta\xi^{(1)}}(xc_{i+1,j}-xc_{i,j}), \tag{42}$$

where (xc, yc) is the co-ordinate of cell centre in the physical space.

Then the predictor of the flow vector is obtained as follows:

$$\tilde{u}^{(1)}_{i,j}=u^{(1)}_{i,j}+(\mathrm{CON}^{(1)}+\mathrm{PRE}^{(1)}+\mathrm{DIF}^{(1)}+\mathrm{EXT}^{(1)})*\Delta t. \tag{43}$$

The second step of the algorithm is the solution of the Poisson equation of pressure. The pressure is defined at the cell centre and the discretization at (i, j) are presented below. The Poisson equation obtained from equation (22b) and $\tilde{u}$ of equation (43) is expressed as follows:

$$\frac{\Delta tV}{\rho}g^{(jk)}\partial_{(j)}\partial_{(k)}\tilde{p}=-h_i\partial_{(i)}\left(\frac{V}{h_i}\tilde{u}^{(i)}\right), \tag{44}$$

where $\tilde{p}$ is the increment of pressure. The above equation is expanded as follows:

$$\frac{\Delta tV}{\rho}(g^{(11)}\partial_{(1)}\partial_{(1)}\tilde{p}+g^{(12)}\partial_{(1)}\partial_{(2)}\tilde{p}+g^{(21)}\partial_{(2)}\partial_{(1)}\tilde{p}+g^{(22)}\partial_{(2)}\partial_{(2)}\tilde{p})$$
$$=-\left[h_1\partial_{(1)}\left(\frac{V}{h_1}\tilde{u}^{(1)}\right)+h_2\partial_{(2)}\left(\frac{V}{h_2}\tilde{u}^{(2)}\right)\right]. \tag{45}$$

The right-hand side of equation (45) is discretized as follows:

$$h_i\partial_{(i)}\left(\frac{V}{h_i}\tilde{u}^{(i)}\right)=\left[\left(\frac{V}{h_1}\tilde{u}^{(1)}\right)_{i+1/2,j}-\left(\frac{V}{h_1}\tilde{u}^{(1)}\right)_{i-1/2,j}+\left(\frac{V}{h_2}\tilde{u}^{(2)}\right)_{i,j+1/2}-\left(\frac{V}{h_2}\tilde{u}^{(2)}\right)_{i,j-1/2}\right]. \tag{46}$$

The first two terms in the parenthesis on the left-hand side equation (45) are taken as examples of discretization and are written, respectively, as follows:

$$g^{(11)}\partial_{(1)}\partial_{(1)}\tilde{p}=\frac{g^{(11)}}{(\Delta\xi^{(1)})^2}(\tilde{p}_{i+1,j}-2\tilde{p}_{i,j}+\tilde{p}_{i-1,j}), \tag{47a}$$

$$g^{(12)}\partial_{(1)}\partial_{(2)}\tilde{p}=\frac{g^{(12)}}{4\Delta\xi^{(1)}\Delta\xi^{(2)}}(\tilde{p}_{i+1,j+1}-\tilde{p}_{i+1,j-1}-\tilde{p}_{i-1,j+1}+\tilde{p}_{i-1,j-1}). \tag{47b}$$

Then the variables in the advanced time step are given by the following forms:

$$p^{\text{new}} = p + \tilde{p}, \tag{48a}$$

$$u^{(1)\text{new}} = \tilde{u}^{(1)} - \frac{\Delta t}{\rho}(g^{(11)}\partial_{(1)}\tilde{p} + g^{(12)}\partial_{(2)}\tilde{p}). \tag{48b}$$

Equation (48b) has differentials and is discretized as follows:

$$u_{\tilde{i},j}^{(1)\text{new}} = \tilde{u}_{\tilde{i},j}^{(1)} - \frac{\Delta t}{\rho}\left[\frac{g^{(11)}}{\Delta\xi^{(1)}}(p_{i+1,j} - p_{i,j}) + \frac{g^{(12)}}{4\Delta\xi^{(2)}}(p_{i+1,j+1} + p_{i,j+1} - p_{i+1,j-1} - p_{i,j-1})\right] \tag{49}$$

The third step of the algorithm is the movement of free surface and the assessment of the impact of grid movement. The movement of free surface is defined at the grid points of the surface leaf and is given from equation (30) as follows:

$$\Delta\xi_{\tilde{i}}^{(2)} = (w_{i,\overline{jj1}}u_{i,\overline{jj1}}^{(2)} + w_{i+1,\overline{jj1}}u_{i+1,\overline{jj1}}^{(2)})\Delta t, \tag{50}$$

where $\overline{jj1}$ is a pointer of the cell face of the surface cell and w is the weight of average, which is inversely proportional to the mesh size. By the weight, the movement of the free surface conserves mass, as illustrated in Figure 3. In this figure, the area of $\triangle$ABK is equal to the area of $\triangle$KCD, $\triangle$KDL to $\triangle$LEF, $\triangle$LFM to $\triangle$MGH and $\triangle$MHN to $\triangle$NIJ; therefore, the total area below the broken line is equal to that below the step drawn with a solid line.

The Lie derivative term of equation (31a) is expanded as follows:

$$u^{(1)}(\text{a}) = u^{(i)}(\text{b}) + (V^{(1)}\nabla_{(1)}u^{(1)} + V^{(2)}\nabla_{(2)}u^{(1)} - \Gamma_{(t1)}^{(1)}u^{(1)} - \Gamma_{(t2)}^{(1)}u^{(2)})\Delta t. \tag{51}$$

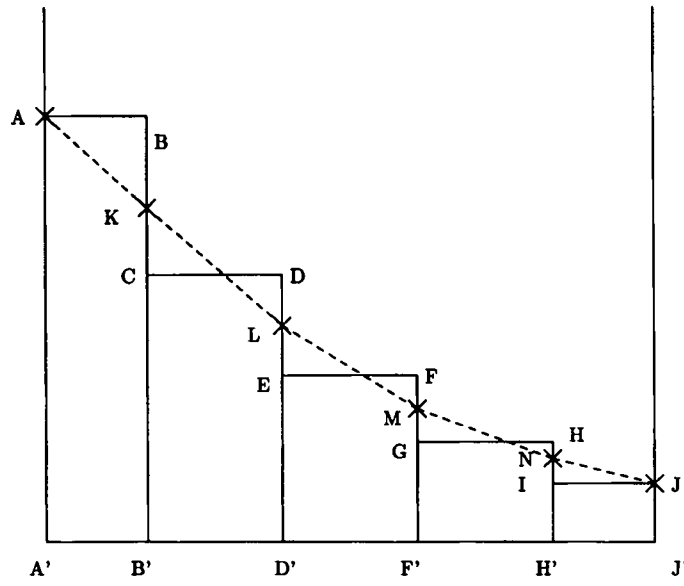

Figure 3. Definition of a free surface: —— result computation; ---- free surface

The initial two terms of the Lie derivative in equation (51) have covariant derivatives, and are discretized as follows:

$$\mathrm{LIE}^{(1)}=\frac{V^{(1)}_{\bar{i},j}}{2\Delta\xi^{(1)}}[(\bar{u}^{(1)}_{\bar{i}+1,j}-\bar{u}^{(1)}_{\bar{i}-1,j})-\mathrm{sgn}(V^{(1)}_{\bar{i},j})(u^{(1)}_{\bar{i}+1,j}-2u^{(1)}_{\bar{i},j}+\bar{u}^{(1)}_{\bar{i}-1,j})]$$
$$+\frac{V^{(2)}_{\bar{i},j}}{2\Delta\xi^{(2)}}[(\bar{u}^{(1)}_{\bar{i},j+1}-\bar{u}^{(1)}_{\bar{i},j-1})-\mathrm{sgn}(V^{(2)}_{\bar{i},j})(u^{(1)}_{\bar{i},j+1}-2u^{(1)}_{\bar{i},j}+\bar{u}^{(1)}_{\bar{i},j-1})] \tag{52}$$

where $\mathrm{sgn}(V)$ assures that these derivatives are assessed in the cell where the mesh moves in.

4.3. Initial and boundary conditions

No turbulence model nor wall function is incorporated yet, because the principal objective of the present paper is the theoretical development and the demonstration of basic performance. To avoid the excessive drag by walls, free-slip condition is applied to the boundaries.

SMAC is an explicit scheme and the time step is limited by the Coulant number. Direct Lagrangian tracking of the free surface circumvents the reduction of time step required by the convergence of VOF value. The stability of free surface can reduce the time step, but a fixed time step of half the Coulant number never causes instability in the following examples.

5. NUMERICAL EXAMPLES

Although the numerical method has been developed in the general 3D form, examples given in this section are performed in 2D to show the basic performance of the present method.

5.1. Surface oscillation initiated by a pressure spike

The first example is chosen to demonstrate the computability of oscillatory free-surface motion initiated by external excitation. A two-dimensional rectangular vessel of width of 4·8 units is filled by liquid to a height of 4·0 units. The fluid has a unit density and a viscosity of 0·01. The surface tension is not specified. A unit gravity acceleration works downwards. A spike of cosine pressure pulse of unit strength in the first mode initiates the oscillation of the free surface. This bench-mark problem was first proposed by Harlow and Welch,[21] who analysed the problem with the marker-and-cell (MAC) method. Later, this problem was analysed by Ramaswamy and Kawahara[2] with the Lagrangian FE Method using 960 elements. In the present work, the problem is analysed with the PCBFC method using 120 cells with the central difference scheme. Free-slip condition is imposed on the walls. A certain $\xi^{(1)}$ axis tracks the free surface and the other $\xi^{(1)}$ axes move in a manner proportional to the movement of the surface grids above them. $\xi^{(2)}$ axes are fixed and parallel to the y axes.

The computed free surfaces and flows of the initial period are shown in Figure 4, with the corresponding pressure contours in Figure 5. These figures show curved free surfaces formed by non-linear effects. Both the free surfaces and the pressure contours show close agreement with those obtained by Ramaswamy and Kawahara. The amplitudes of a spike (higher end) and a bubble (lower end) of the free surface in its initial half period are shown in Figure 6, along with those obtained by Harlow and Welch[2] for comparison. Both the spike and the bubble show good agreement, but the period of oscillation is shorter by a small amount than that of Harlow and Welch.

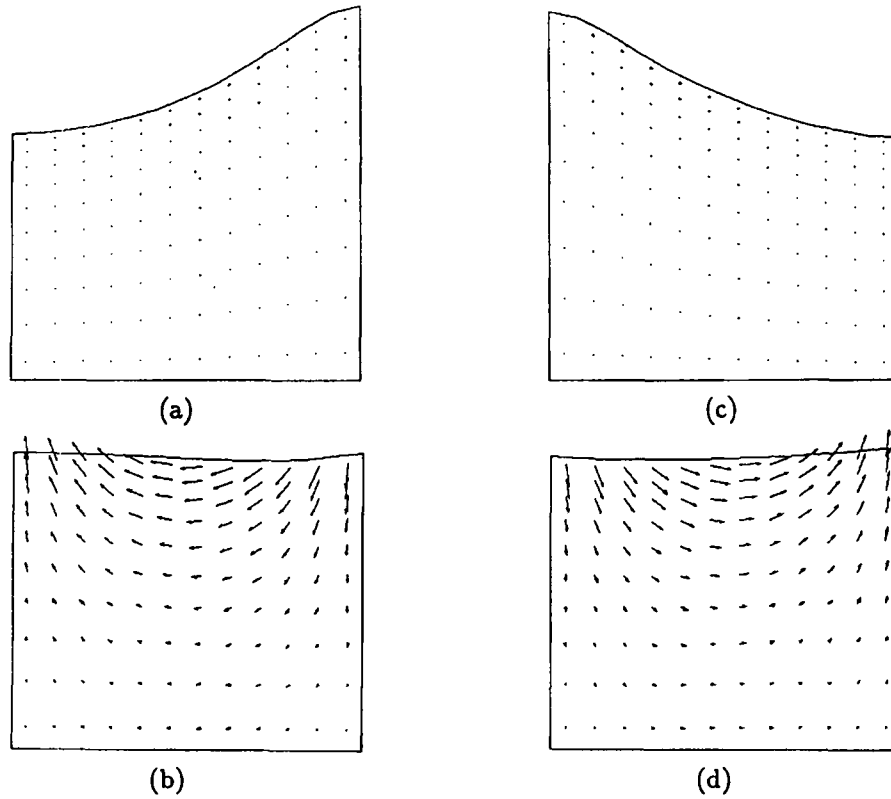

Figure 4. Oscillation of the free surface and the inside flow initiated by a pressure spike: (a) $t=2{\cdot}0$; (b) $t=4{\cdot}0$; (c) $t=6{\cdot}0$; (d) $t=8{\cdot}0$

The potential energy can be assessed by summing up the potential energies of all the cells and is expressed as follows:

$$\tilde{E}_{\text{pot}}(t)=\sum\{1/6\Delta x[(y_4^2+y_3^2+y_3y_4)-(y_2^2+y_1^2+y_1y_2)]\}, \tag{53a}$$

where Δx, y_1 and y_2, and y_3 and y_4 are the width of cell, heights of two lower grid points of the cell, and those of two higher grid points of the cell, respectively, and the summation extends to all cells. Then the pure gain of the potential energy is obtained in the following form:

$$E_{\text{pot}}=\tilde{E}_{\text{pot}}(t)-\tilde{E}_{\text{pot}}(0), \tag{53b}$$

where $\tilde{E}_{\text{pot}}(0)$ is the base potential energy when the fluid is stationary. The kinetic energy is estimated by the following equation:

$$E_{\text{kin}}=1/2\sum S(u^2+v^2+2uv\cos\alpha), \tag{54}$$

where S, u, v and α are the area of the cell, $u^{(1)}$, $u^{(2)}$, and the angle formed by $\xi^{(1)}$ and $\xi^{(2)}$ axes, respectively. Then the total energy is defined as a sum of the potential energy and the kinetic energy:

$$E_{\text{tot}}=E_{\text{pot}}+E_{\text{kin}}. \tag{55}$$

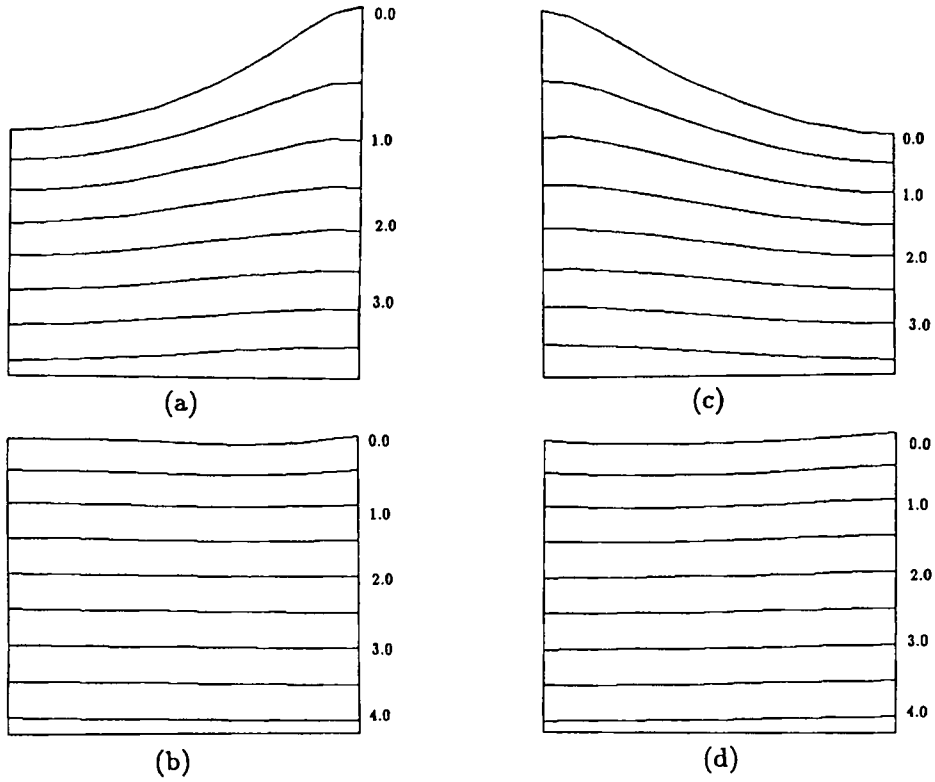

Figure 5. Pressure contours corresponding to Figure 4

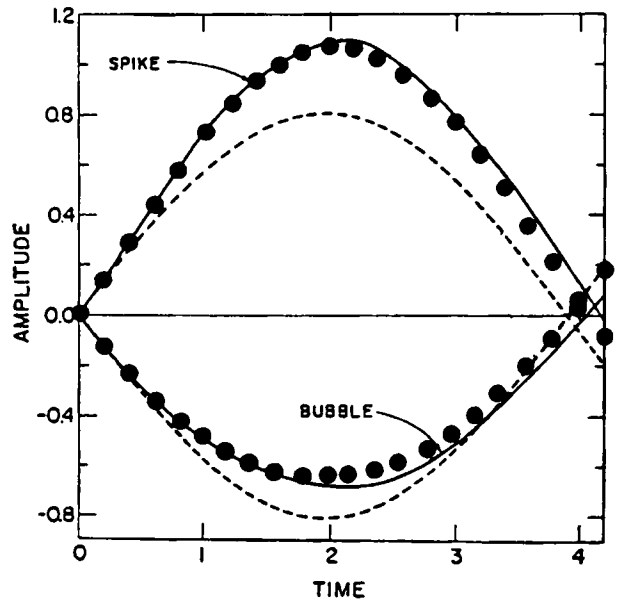

Figure 6. Amplitude of a spike and a bubble (drawn on the figure of Reference 21): —— computation by SMAC, ● computation by PCBFC, ---- prediction of linear theory

The above definition ignores the contribution of pressure, because the pressure is known only at the cell centre and the total pressure may cause relatively large numerical errors when the basic pressure before the initiation of oscillation is subtracted.

Figures 7(a) and 7(b) show the history of free-surface amplitudes and that of energies for the initial five periods. Both the amplitudes and the energies show gradual decreases by the viscosity of the fluid. The decrease of amplitudes shows small fluctuation at the spike, presumably because of the large distortion of cells; this may be improved by a modification of the boundary conditions or the convective scheme. The decrease of energy shows no fluctuation. A small periodical oscillation of the total energy in this closed system may be attributed to the omission of pressure from the definition.

5.2. Free-surface motion under forced circulation

The second example is chosen to demonstrate the computability of free-surface motion induced by forced circulation. The experiment of this bench-mark was performed by Ueda *et al.*[22] for the basic study of free-surface motion of the coolant of a liquid-metal-cooled fast breeder reactor

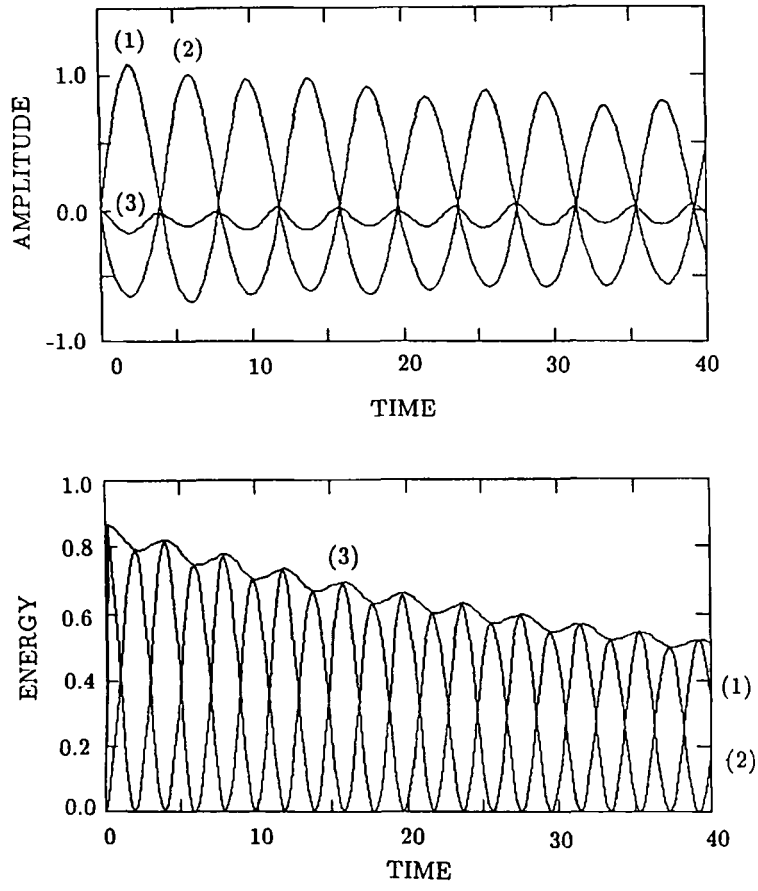

Figure 7. History of amplitudes and energy corresponding to Figure 4. (a) History of amplitudes: (1) right end; (2) left end; (3) centre. (b) History of energy: (1) kinetic energy; (2) potential energy; (3) total energy (pressure is not added)

(LMFBR). The experimental section is a rectangular tank of width of 2·0 m, height of 2·0 m and thickness of 0·1 m. It is initially filled with water to a height of 1·7 m. The experimental section had an inlet at the left end of the bottom, guide board of the injection flow along the left wall, and an outlet near the lower end of the right wall. Both the inlet and outlet have a width of 0·2 m. Water was circulated from the outlet to the inlet through a closed piping system to keep an average water level of the tank. The case of injection velocity 1·0 m/s is chosen for the analysis. The analysis is performed with 324 cells. Each cell has a size of 0·1 m by 0·1 m, except for those in the top two layers, that have only half the heights, to have a high resolution of flow near the free surface. A certain $\xi^{(1)}$ axes tracks the free surface, and only the upper half of $\xi^{(1)}$ axes move with the free surface in a manner proportional to the movement of the free surface. $\xi^{(2)}$ axes are fixed and parallel to the y axes. The upstream difference scheme is used and the free-slip condition is imposed on the walls.

Figure 8 exhibits the computed free surface and the flow after 30 s of water injection. The flow is developed and the free surface shows little movement at 30 s. The centre of the free surface is lower than both the ends, which is formed by the difference of dynamic pressure. Figure 9 shows a comparison of the calculated free surface and flow vectors with the experimental observations. A small swell of water level that was caused by inevitable gas entrainment at the free surface was observed in the experiment; the computed free surface was lifted by approximately 2 cm so that the surface height at 700 mm from the left wall met with that of the experimental observations. The change of water level may have effects on the flow and the free surface in a strict sense, but as the lifted height is very small compared to the water level of the fluid and there is no structure near the free surface such as inlet or outlet that is influential on the flow pattern, it is assumed that the effect of the lifting is small. The agreement of the shape of the free surface is fairly good. Flow vectors also show fairly good agreements except for the one just above the injection port, where the injected water hits the surface and there is a large gradient of flow velocity. These agreements will be improved by a high-ordered convective scheme with low numerical viscosity. The computation showed no numerical instability even in the case of the maximum experimental injection velocity of 1·6 m/s, in which case the free surface observed in the experiment was rough, with uncountable bubbles of entrained air below it.

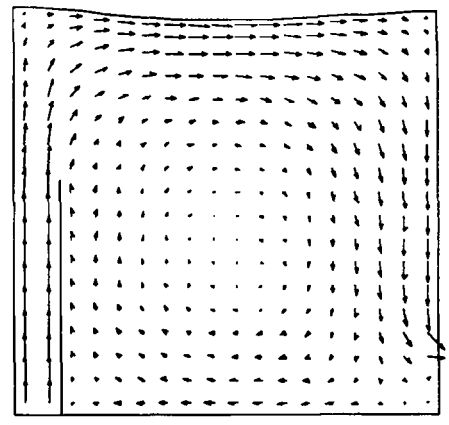

Figure 8. Free surface and inside flow formed by forced circulation (1·0 m s^{-1} of injection velocity)

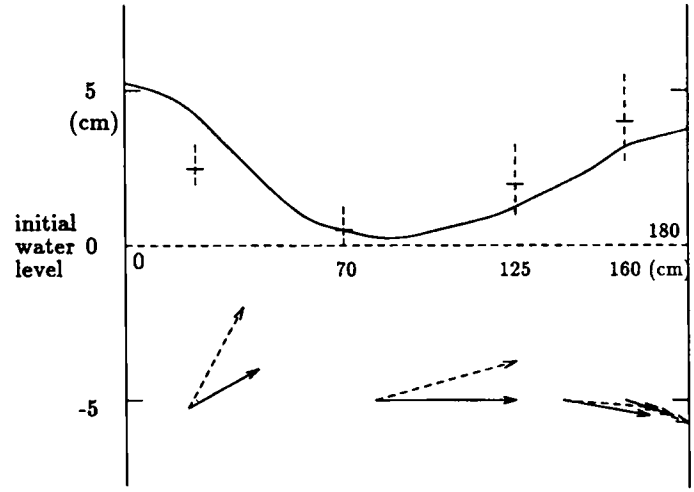

Figure 9. Comparison of surface heights and flow vectors of Figure 8 with the experimental observations: —— computation; ---- experiment

5.3. *Circulation-coupled periodical sloshing*

The third example is chosen to demonstrate the computability of the complex free-surface motion of circulation-coupled periodical sloshing. Constantly circulated free-surface flow shown in Figure 8 is set under external excitations. First, a cosine pressure pulse in the first mode, just as used in Section 5.1, is applied on the free-surface flow of Figure 8 to find the natural period of sloshing. The computed period of sloshing is 1·64 s, a little longer than 1·50 s that is the period of pure sloshing without circulation. Elongation of the period under circulation has been experimentally observed by Hara.[23] Then the free surface flow of Figure 8 is shaken horizontally by a sinusoidal acceleration of 0·01 G with the natural period of sloshing.

The computed free surfaces after being shaken for four periods are shown in Figure 10. No numerical instability is seen at the free surface nor at the flow. A wave separates from a spike at the downstream in Figure 10(a), propagates towards the upstream in Figure 10(b) and is absorbed timely into a spike at the upstream in Figure 10(c). No wave is observed in Figure 10(d), but a hollow is seen at the centre. In Figure 10(a) the spike is at the highest but the bubble is a little before the lowest moment. In Figure 10(c) the spike is at the highest but the bubble is a little after the lowest moment. The wave propagation and the shift of timing between the two ends of the free surface have been experimentally observed by Okamoto *et al.*[24] In spite of the complex movement of the free surface, the movement of the grid is minimized by the extension of the PCBFC method to the general non-orthogonal grids.

Computation of the problem of the Section 5.1 for five periods takes 20 s, and those of Sections 5.2 and 5.3 for 30 s take 30 s of CPU time with the Hitac M-682 of the Computer Center in the University of Tokyo. Approximately 30% of the total computation time is consumed by the assessment of the terms intrinsic to the PCBFC method and the grid movement.

6. CONCLUSIONS

The characteristics of incompressible fluid flow analysis based on physical component in the non-physical BFC method were clarified and the generalized formulation of this method that should be understood as a physical curvilinear BFC (PCBFC) method was presented based on

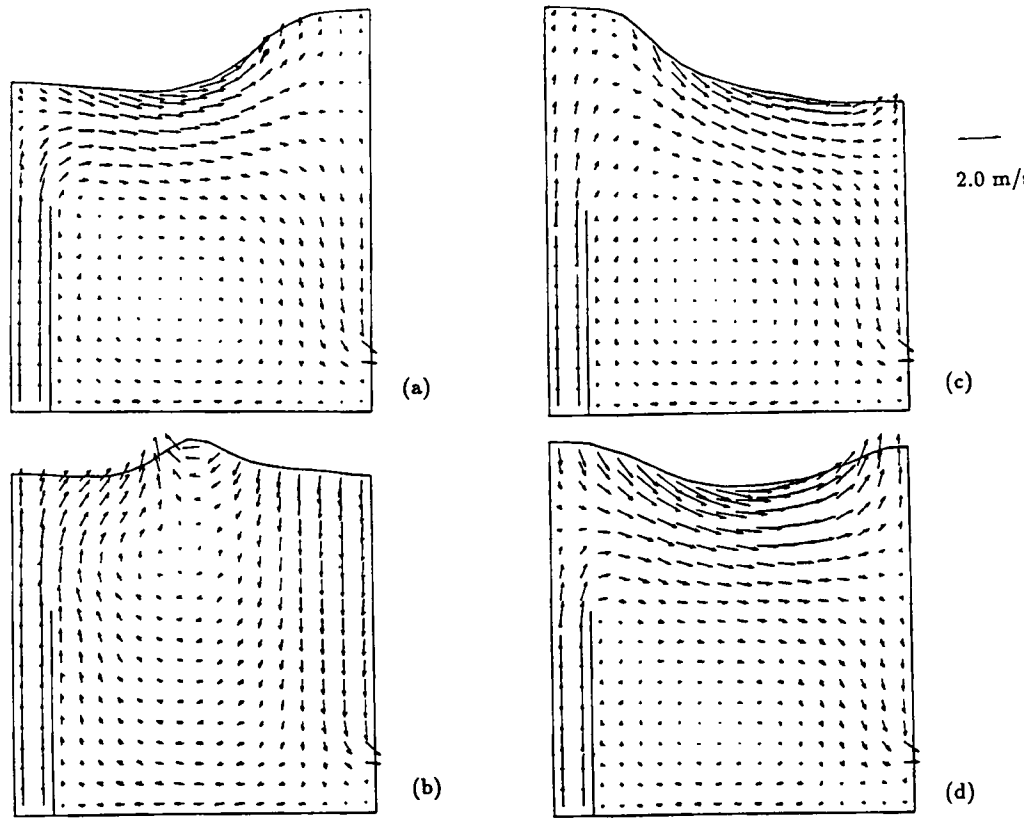

Figure 10. Free surface and the inside flow formed by circulation-coupled sloshing: (a) right end highest; (b) wave propagation; (c) left end highest; (d) centre fall

the theory of Riemannian geometry. The usefulness of the governing equations of fluid flow and free-surface motion that were described in the form of PCBFC was validated by analysing several cases of free-surface flow. The formulation in this paper is very general and its applicability is not confined only to the analysis of free-surface motion. Research is currently under way to demonstrate the wider applicability of PCBFC method by developing a tool for 3D analysis with moving boundary.

APPENDIX

The basic concepts of differential geometry and the manifold theory[17–19] related to the main body of the present paper are summarized.

A.1. Metric

A Riemannian metric on a space M is a tensor field g of type (0, 2) (covariant tensor of level 2) on M subject to the conditions:

(i) g is symmetric, i.e. $g_{ij}=g_{ji}$, and
(ii) g is positive-definite, i.e. $g_{ij}x^i x^j>0$:

$$g_{(ij)}=T^i_{(i)}T^j_{(j)}g_{ij}, \tag{56}$$

where T is a transformation matrix defined by equation (60). Metric is a tensor that defines the length on M. Given the metric, a length s of a parametrized curve $x=c(t)$ is defined by the following integral:

$$s=\int_{t0}^{t1}(g_{ij}\dot{x}^i\dot{x}^j)^{1/2}\,\mathrm{d}t, \tag{57a}$$

where the curve is parametrized from $t0$ to $t1$ and the over dot denotes differentiation with respect to t:

Euclidean space has a trivial metric

$$g_{ij}=\delta_{ij}, \tag{58}$$

where δ_{ij} is the Kronecker symbol. With the metric of equation (58), equation (57a) reduces to the following form:

$$s=\int_{t0}^{t1}[\sum(\dot{x}^i)^2]^{1/2}\,\mathrm{d}t, \tag{57b}$$

which is the formula that defines the length in the Euclidean space based on the Pythagoras' theorem.

A.2. Connection and covariant derivative

Partial derivatives of a function f with respect to given systems of local co-ordinates on a space M are the components of a tensor field:

$$\frac{\partial f}{\partial \xi^j}=T_j^{(j)}\frac{\partial f}{\partial \xi^{(j)}}, \tag{59}$$

where ξ^j and $\xi^{(j)}$ are the systems of the local co-ordinates and $T^j_{(j)}$ are the members of transformation matrix

$$T_j^{(j)}=\frac{\partial \xi^{(j)}}{\partial \xi^j}. \tag{60}$$

A similar computation for the contravariant vector field u^i, which satisfies

$$u^i=T^i_{(i)}u^{(i)},$$

results in

$$\frac{\partial u^i}{\partial \xi^j}=T_j^{(j)}\left(T^i_{(i)}\frac{\partial u^{(i)}}{\partial \xi^{(j)}}+\partial_{(j)}(T^i_{(i)})u^{(i)}\right). \tag{61}$$

The presence of the second term in the parentheses on the right-hand side of the above equation indicates that the derivative of a covariant vector field does not have a tensor character. The derivative of a covariant vector field may be given an invariant (co-ordinate-free) meaning by introducing a set of n^3 'connection coefficients' Γ^i_{jk}, which satisfiy the following equation

$$\Gamma^i_{jk}=T^i_{(i)}[\Gamma^{(i)}_{(jk)}T_j^{(j)}T_k^{(k)}+\partial_j(T_k^{(i)})], \tag{62}$$

as it transforms equation (61) into the following form:

$$\left(\frac{\partial u^i}{\partial \xi^j}+\Gamma^i_{jk}u^k\right)=T^i_{(i)}T_j^{(j)}\left(\frac{\partial u^{(i)}}{\partial \xi^{(j)}}+\Gamma^{(i)}_{(jk)}u^{(k)}\right). \tag{63}$$

Equation (63) means that a covariant derivative of u^i with respect to ξ^i, $\nabla_j u^i$, which is defined by

$$\nabla_j u^i = \frac{\partial u^i}{\partial x^j} + \Gamma^i_{jk} u^k, \tag{64}$$

transforms like a tensor field of type (1, 1). We can also represent the operator ∇ by giving its action on basis vector fields $(e_j)=(\partial/\partial\xi^j)$ as follows:

$$\nabla_{e_j} e_k = \Gamma^i_{jk} e_i. \tag{65}$$

Note that the connection coefficient itself is not a tensor. From equation (59), the covariant derivative of a function f is identical to its partial derivative,

$$\nabla_j f = \frac{\partial f}{\partial \xi^j}. \tag{66}$$

The Euclidean space has a trivial connection, that is,

$$\Gamma^i_{jk} = 0 \quad \text{(Euclidean space)}. \tag{67}$$

A.3. Parallelism

A vector at P and one at Q of a space M are said to be parallel if they are identified with the same vector at some point on M. By definition, vectors $u^i(t)$ are parallel along a curve $C(t)$ if the covariant derivative of $u^i(t)$ vanishes in the direction of $C(t)$, that is, if the following equations holds in the direction of $C(t)$:

$$\frac{\partial u^i}{\partial t} + \Gamma^i_{jk} \frac{\mathrm{d}\xi^k}{\mathrm{d}t} u^j = 0. \tag{68}$$

This definition is co-ordinate-independent, but may well be path-dependent. Equation (68) shows that the connection defines parallelism (local direction) of a space.

A.4. Lie derivative

The geometric operation measuring the change of geometrical objects by a given transformation is called the 'Lie derivative'. The Lie derivative of u^i with respect to the vector field V at point q, $\mathrm{L}_V u^i$ is defined as follows:

$$\mathrm{L}_V u^i = \lim \frac{\phi^* u^i(q+\varepsilon) - u^i(q)}{\varepsilon}, \tag{69}$$

where $u^i(q+\varepsilon)$ is u^i at the point proceeded by ε along the field V from the point q and ϕ^* is a pullback operation. For the contravariant vector u^i, equation (69) is calculated as the following:

$$\mathrm{L}_V u^i = V^j \frac{\partial u^i}{\partial \xi^j} - u^j \frac{\partial V^j}{\partial \xi^j}, \tag{70}$$

or, in a general space,

$$\mathrm{L}_V u^i = V^j \nabla_j u^i - u^j \nabla_j V^i. \tag{71}$$

The Lie derivative of a function f is given as

$$\mathrm{L}_V f = V^j \nabla_j f = V^j \frac{\partial f}{\partial \xi^j}. \tag{72}$$

A.5. Metrical connection

A connection compatible with a metric is called a 'metrical connection'. Compatibility demands that the inner product of two vectors that are parallel-transported be constant:

$$\nabla_k g_{ij}=0. \tag{73}$$

In other words, metrical connection conserves lengths and angles under parallel transport.

A.6. Torsion and curvature

Geometrical structure of a space can be represented by the invariants of connection. These invariants are the torsion and the curvature. The former is an invariant that depends on connection, while the latter is independent of connection and a local invariant of a space.

Consider a small circuit (right square) drawn parallel and a vector that is parallel-transported along the circuit. The circuit on a general space does not necessarily close, nor is the transported vector identical to the original one, suffering twist. The failure of a circuit to close is expressed by torsion. Torsion T is represented by an operator $T(X,Y)$ that takes in two vectors X and Y, representing the sides of the circuit, and yields the mismatch factor. By calculation, this operation is obtained as follows:

$$T(X, Y)=\nabla_X Y-\nabla_Y X-[X, Y], \tag{74}$$

where $\nabla_X Y$ is a covariant derivative of Y in the direction of X,

$$\nabla_X Y^i=X^j\nabla_j Y^i, \tag{75}$$

and $[X, Y]$ is a Lie bracket,

$$[X, Y]^i=X^j\partial_j(Y^i)-Y^j\partial_j(X^i). \tag{76}$$

Its components are given by the following form:

$$T^i_{jk}=\Gamma^i_{jk}-\Gamma^i_{kj}. \tag{77}$$

Torsion is a tensor of type (1, 2).

The twist of a parallel-transported vector, or the path dependence of a parallel-transported vector is reflected on the curvature R. R is represented by an operator $R(X, Y)Z$ that takes in X and Y, representing the sides of the circuit, and Z the vector transported around the circuit, and yields the twist vector. Calculation shows that this operation can be written in a manifestly covariant form,

$$R(X, Y)Z=[\nabla_X, \nabla_Y]Z-\nabla_{[X, Y]}Z. \tag{78}$$

Its components are given by

$$R^i_{jkl}=\partial_k\Gamma^i_{jl}-\partial_l\Gamma^i_{jk}+\Gamma^m_{il}\Gamma^i_{mk}-\Gamma^m_{jk}\Gamma^i_{ml}. \tag{79}$$

Curvature is a tensor of type (1, 3). A curvature-free space supports global (absolute) direction defined on the space.

A.7. Foliation

A space (n-dimensional manifold) M is said to have a 'k-dimensional foliation', defined on it if it is 'foliated' into k-dimensional surfaces, i.e. if for each point of M there is one and only one smooth

k-dimensional subspace passing through that point in a manner depending smoothly on the point of the space:

$$\bigcup L_\alpha = M \quad \text{and} \quad L_\alpha \cap L_\beta = \varnothing \quad (\alpha \neq \beta), \tag{80}$$

where L_α are the specified surfaces and are called the 'leaves' of the foliation. It is further required that in some neighbourhood of each point of M there can be introduced co-ordinates $x^1, \ldots, x^k, y^1, \ldots, y^{n-k}$ with the properties that the level surfaces $y^1 = a_1, \ldots, y^{n-k} = a_{n-k}$ are just the leaves of the foliation in that neighbourhood and that $x^1, \ldots, x^k$ are local co-ordinates for each leaf:

$$L_\alpha = (x^i, y^j) \quad \text{such that} \quad y^j = a_j. \tag{81}$$

REFERENCES

1. B. D. Nichols, C. W. Hirt and R. Hotchkiss, 'SOLA-VOF: a solution algorithm for transient fluid flow with multiple free surface', *LA-8355* (1980).
2. B. Ramaswamy and M. Kawahara, 'Lagrangian finite element analysis applied to viscous free surface fluid flow', *Int. j. numer. methods fluids*, **7**, 953–984 (1987).
3. D. Medina, J. Liggett, A. Birchwood and K. Torrence, 'A consistent boundary element method for free surface hydrodynamic calculations', *Int. j. numer. methods fluids*, **12**, 835–857 (1991).
4. H. J. Haussling and R. M. Coleman, 'Nonlinear water waves generated by an accelerated circular cylinder', *J. Fluid Mech.*, **92**, 761–781 (1979).
5. C. Truesdell, 'The physical component of vectors and tensors', *Z. Angew. Math. Mech.*, **33**, 345–356 (1953).
6. S. B. Pope, 'The calculation of turbulent recirculating flows in general orthogonal coordinates', *J. Comput. Phys.*, **26**, 197–217 (1978).
7. G. Ryskin and L. G. Leal, 'Orthogonal mapping', *J. Comput. Phys.*, **50**, 71–100 (1983).
8. G. Ryskin and L. G. Leal, 'Numerical solution of free boundary problems in fluid mechanics', *J. Fluid Mech.*, **148**, 1–43 (1984).
9. I. Demirdzic, A. D. Gosman, R. I. Issa and M. Peric, 'A calculation procedure for turbulent flow in complex geometries', *Comput. Fluids*, **15**, 251–273 (1987).
10. S. Koshizuka, Y. Oka and S. Kondo, 'A staggered differencing technique on boundary-fitted curvilinear grid for incompressible Navier–Stokes equation written with physical components', in A Collection of Technical Papers; 3rd International Symposium on Computational Fluid Dynamics, Nagoya, Japan (1989).
11. S. Koshizuka, Y. Oka and S. Kondo, 'A boundary-fitted staggered difference method for incompressible flow using Riemann geometry', in *Proc. 1st Int. Conf. on Supercomputing in Nuclear Applications*, Mito, Japan (1990).
12. S. Koshizuka, Y. Oka and S. Kondo, 'A staggered differencing tecnhique on boundary-fitted curvilinear girds for incompressible flows along curvilinear or slant walls', *J. Comput. Mech.*, **7**, 123–136 (1990).
13. S. Koshizuka and Y. Oka, 'A calculation procedure of coordinate free Navier–Stokes equations on boundary-fitted grids', in *Proc. Num. Meths. Laminar Turbulent Flow*, Stanford, U.S.A. (1991).
14. S. Ogawa and T. Ishiguro, 'A method for computing flow fields around moving bodies', *J. Comput. Phys.*, **69**, 49–68 (1987).
15. A. Takizawa and S. Kondo, 'Development of a BFC method without non-physical quantity and incorporation of Lie derivative for grid-moving problems', in *The 3rd Symposium on CFD*, Tokyo, Japan (1989) (in Japanese).
16. R. Aris, *Vectors, Tensors, and the Basic Equations of Fluid Dynamics*, Dover, New York, 1989.
17. S. I. Goldberg, *Curvature and Homology*, Dover, New York, 1982.
18. W. L. Burke, *Applied Differential Geometry*, Cambridge University Press, Cambridge, 1985.
19. B. A. Dubrovin, A. T. Fomenko and S. P. Novikov, *Modern Geometry—Methods and Applications, Part II. The Geometry and Topology of Manifolds*, Springer, Berlin, 1985.
20. A. Amsden and F. H. Harlow, 'The SMAC method: a numerical technique for calculating incompressible fluid flow', *LA 4370* (1970).
21. F. H. Harlow and J. E. Welch, 'Numerical study of large-amplitude free-surface motions', *Phys. Fluids*, **9**, 842–851 (1966).
22. H. Ueda, A. Takizawa, H. Terasaka, N. Shirakawa and K. Ogura, 'Experimental investigation on free surface movement of pool type FBRs', in *Proc. Int. Conf. on Fast Reactor and its Fuel Cycles*, Kyoto, Japan (1991).
23. F. Hara, 'Experimental study on sloshing characteristics of a flowing liquid in a tank', *Pressure Vessels Pipings*, **157**, 133–141 (1989).
24. K. Okamoto, H. Madarame and T. Hagiwara, 'Self-induced oscillation of free surface in a tank with circulating flow', in *Proc 5th Int. Conf. on Flow Induced Vibration*, IMechE 1991-6, 539–545 (1991).